Low-dimensional magnetism in multivariate copper/zinc MOF-74 materials formed via different mechanochemical methods †

Senada Muratović,[‡,△] Valentina Martinez,[‡,△] Bahar Karadeniz,[‡] Damir Pajić,[¶] Ivana Brekalo,[‡] Mihails Arhangelskis,[§] Matjaž Mazaj,[‖] Gregor Mali,[‖] Martin Etter,[⊥] Tomislav Friščić,[#] Yulia Krupskaya,[@] Vladislav Kataev,[@] Dijana Žilić,[*,‡] and Krunoslav Užarević[*,‡]

‡*Ruđer Bošković Institute, Bijenička cesta 54, 10000 Zagreb, Croatia.*
¶*University of Zagreb, Faculty of Science, Department of Physics, Bijenička cesta 32, 10000 Zagreb, Croatia.*
§*Faculty of Chemistry, University of Warsaw, 1 Pasteura St, 02-093 Warsaw, Poland.*
‖*National Institute of Chemistry, Hajdrihova 19, SI-1001 Ljubljana, Slovenia.*
⊥*Deutsches Elektronen-Synchrotron DESY, Notkestraße 85, D-22607 Hamburg, Germany.*
#*McGill University, Montreal, Quebec H3A 0B8, Canada.*
@*Leibniz IFW Dresden, Helmholtzstrasse 20, D-01069 Dresden, Germany.*
△*equally contributing first authors*

Received August 12, 2022; E-mail: dijana.zilic@irb.hr; krunoslav.uzarevic@irb.hr

Abstract: MOF-74 are an archetypal magnetic metal-organic framework (MOF) family, with metal nodes bridged by 2,5-dioxido-1,4-benzenedicarboxylic acid (H_4dobdc), and arranged into one of the simplest representations of 1D Ising magnetic model. Recently, a novel mechano-synthetic approach opened a pathway towards a series of bimetallic multivariate (1:1) M1M2-MOF-74 materials, with the uniform distribution of metal cations in the oxometallic chains, offering a unique opportunity to investigate low-dimensional magnetism in these heterometallic MOFs. We explore here how different mechanochemical procedures affect the interaction between the metal nodes of the model system of three multivariate copper(II)/zinc(II)-MOF-74 materials, two of which were obtained through a template-controlled procedure, and the third one was obtained by recently developed mechanical MOF-alloying combined with subsequent accelerated aging. While the three Cu/Zn-MOF-74 products have almost identical PXRD diffractograms and FTIR spectra, they differ significantly in their magnetic properties, as revealed through detailed magnetization, and X-band and multifrequency high-field ESR measurements. The magnetic results of the three multivariate Cu/Zn-MOF-74s were compared to the properties of monometallic Cu-MOF-74, which shows antiferromagnetic intra-chain and weaker ferromagnetic inter-chain interaction. EDAX/SEM and solid-state NMR spectroscopy helped rationalize the observed differences in magnetization, and in-situ synchrotron PXRD monitoring of templated MOF formation revealed different reaction pathways when using the zinc or copper intermediates, involving even the fleeting occurrence of a rare MOF-74 polymorph.

INTRODUCTION

Thirty years after their discovery, metal-organic frameworks (MOFs), porous coordination polymers comprised of metal nodes bridged by organic molecules, are still widely considered "novel" materials as this field remains one of the fastest developing and studied fields in materials chemistry, taking many new directions concerning the composition of MOFs and their applicability.[1–5] One of the sub-fields that attract significant attention are multivariate MOF materials containing diverse metal nodes in the MOF structure, but these materials are still scarce.[6–8] Such disparity in the multivariate-MOF classes stems from the difficulty of controlling the uniformity of distribution and the relative ratio of the respective metal-node constituents in the two main conventional solvothermal approaches, post-synthetic metal exchange, and direct synthesis.[9] Post-synthetic exchange relies on the soaking of monometallic MOF in a solution containing the salt of the other metal(s), usually for a period of days to weeks.[10,11] The literature on thermodynamic and kinetic factors governing the process is still limited, and the process is hard to control.[12,13] In the direct synthesis approach, MM-MOFs are built from solutions containing linkers and multiple metal salts. While there are several studies where a significant degree of control of metal content in MM-MOFs was obtained through careful choice of the metal source and synthetic/crystallite growth conditions, the inclusion of a respective metal is most often serendipitous.[14–16] This is mostly expected; many factors in the nature of the metal cation (such as the acidity, charge, softness, and radius), solvent effects (solubility, pH, and solvation), and the thermodynamics of the process must be taken into account to introduce a higher degree of control into processing.[7]

A particularly important target for multivariate MM-MOFs is the MOF-74 family, also known as CPO-27.[19] From the first reports, these chemically stable MOFs, characterized by large channels (12 Å diameter) and open metal sites, stood out on account of their outstanding properties.[2,20] In MOF-74, the metal cations are ordered in 1D metal-oxo chain secondary building units (SBUs), bridged by 2,5-dioxido-1,4-benzenedicarboxylate anions ($dobdc^{4-}$) to form M_2(dobdc) MOF with hexagonal channels in a honeycomb arrangement (Figure 1a). They are highly modular and several monometallic M-MOF-74 are known (M = Mg, Zn, Cd, Co, Mn, Fe, Ni, and Cu)[21–23] providing an ideal platform for preparation of mixed metal phases. It is expected that these materials may have unique properties stemming from the synergistic effect between the two metals coupled closely in the 1D oxometallic chain. However, initial attempts at making mixed metal MOF-74 (MM-MOF-74) materials through post-synthetic metal exchange showed that the replacement of the metal cation is not straightforward, and the

†ESI contains Materials and methods, and supporting PXRD, TGA, FTIR, AAS, EDAX/SEM, magnetization and ESR results.

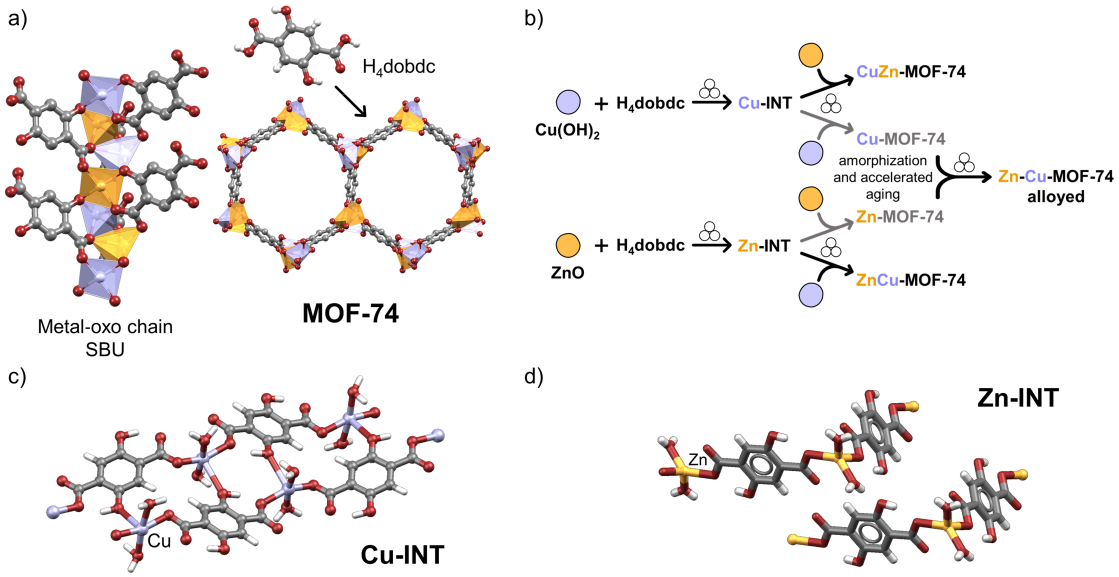

Figure 1. a) Representation of the idealised crystal structure of MM-MOF-74, and its constituents. H_4dobdc linker bridges metal-oxo chains to form the MOF-74 structure with hexagonal channels along the *c*-axis. H atoms of SBU and MOF are omitted for clarity. b) Schematic representation of the mechanochemical synthesis of binary multivariate Cu/Zn MOF-74 materials examined in this study. c) Structure of $[Cu(H_2dobdc)(H_2O)_2]_n$ (Cu-INT) prepared in this study. d) Structure of $[Zn(H_2dobdc)(H_2O)_2]_n$ (Zn-INT) CCDC code: ODIPOH.[17,18] Color code: copper blue, zinc yellow, carbon grey, oxygen red, hydrogen light grey.

reported transmetallation efficiency was low.[24] Nevertheless, even with a low inclusion of the second metal, the obtained materials expressed large advances in their catalytic properties and chemical stability.[7]

Conversely, the direct solvothermal synthesis approach yielded MM-MOF-74 materials with up to 10 different metals incorporated in the framework,[25] but with significant inhomogeneity both in the ratio and distribution of the metal nodes, yielding crystallites with different composition in the same product. The same group reported recently a series of binary MM-MOF-74 materials incorporating Co, Cd, Pb, and Mn, where the atom probe tomography was used to tackle the issue of local distribution of metals in MM-MOFs. It was shown that the occurrence and distribution of metal nodes largely depended on the type of the metal incorporated, and the temperature of the synthesis.[26] It follows that, while the metal-oxo chains in MOF-74 can accommodate different metals in close vicinity - making them a prime target for MM-MOF synthesis - current synthetic approaches lack the needed control and tunability to truly realize the potential of these materials. Therefore, overcoming the limitations of conventional synthetic procedures and the dependence of MM-MOF-74 assembly on judicious choice of metals may have a transformative impact on the field of multivariate MOFs.

Two interesting synthetic alternatives to MM-MOFs rely on mechanochemical processing. The first one is mechanical alloying.[27] Here, the authors dry-milled a mixture containing a pair of monometallic MOFs until no Bragg peaks were detectable by powder X-ray diffraction (PXRD). The amorphous matrix was then exposed to water vapors in an accelerated aging process[28] to obtain crystalline Al/Gd (1,4-naphthalenedicarboxylate). The alloying method was tested for several other archetypal MOFs, including MOF-74, ZIF-8, and HKUST-1. The results showed that the success of alloying largely depends on several parameters involving the ionic radii, coordination preferences, charge and electronegativity of the metal nodes, as well as the MOF topology.

The other mechanochemical method is a two-step process involving monometallic coordination intermediates and ditopic ligands. To the best of our knowledge, it presents the only chemically-controlled approach towards MM-MOFs reported to date, where the different reactivity of the functional groups on the ligand led to controllable coordination and positioning of the two metals in the framework. This two-step mechanochemical strategy circumvented the issues related to solution synthesis, yielding a series of twelve porous, stable, and well-defined 1:1 binary MM-MOF-74 materials with pairs of main and transition metals.[29] In the first step, the first metal and H_4dobdc formed a precursor $[M(H_2dobdc)(solvent)]_n$ through coordination of the reactive carboxylate groups, while the second metal activated the remaining phenolic groups to form highly porous and stable binary MM-MOF-74 products upon further milling, where the position of a particular metal is defined by the order of coordination. From this series, only one MOF was tested for the real-world application so far. While the monometallic zinc or copper MOF-74 materials were inactive, the mixed metal ZnCu-MOF-74 showed dramatically increased catalytic activity towards the selective catalytic formation of methanol from carbon dioxide based on a synergistic action among the zinc and copper nodes.[30]

As one of unique potential applications, the MM-MOF-74 allows for the systematic studying of low-dimensional magnetism in multimetallic systems. These porous magnets have an advantage compared to inorganic materials, such as oxides and polymers, as the targeted synthesis leads to better control of the spatial arrangement and separation of magnetic centers and chains which is much sought for advanced applications. Metal nodes are organized in infinite and efficiently separated 1D chains, making MOF-74 probably the simplest realization of the 1D Ising model.[31] Until now, the magnetic properties of Fe-, Co- and Ni-MOF-74 were studied, revealing a plethora of interesting phenomena such as solvent-exchange induced switching from ferromagnetic (FM) to antiferromagnetic (AFM) state, metamagnetism,

spin-crossover, etc.[20,32–38] To the best of our knowledge, only three heterometallic MOF-74 were studied, none with a defined metal distribution. Rubio-Giménez and collaborators studied the spontaneous magnetization of Ni-MOF-74 upon iron doping ($Ni_{1-x}Fe_x$-MOF-74, x = 4 or 6%),[35] the Zhao group investigated Co_xFe_{1-x}-MOF-74 for its catalytic activity with only ESR spectra presented,[39] and recently, Co_xNi_{1-x}-MOF-74, where x = 0.752, 0.458, and 0.233, were reported.[40]

Here, we present the magnetic properties of three different binary multivariate MM-MOF-74 materials comprised of zinc(II) and copper(II) nodes in a 1:1 ratio (Figure 1b) prepared by different mechanochemical approaches and from different polymeric precursors. As the magnetic properties of monometallic Cu-MOF-74 are unknown, we first thoroughly characterised Cu-MOF-74, followed by the preparation of two bimetallic Cu/Zn materials by a template-controlled approach. Two different coordination M(H_2dobdc) polymers, $[Cu(H_2dobdc)(H_2O)_2]_n$ (Cu-INT) (Figure 1c) and $[Zn(H_2dobdc)(H_2O)_2]_n$ (Zn-INT) (Figure 1d), were used as precursors in the preparation of CuZn-MOF-74 and ZnCu-MOF-74, respectively. A third mixed metal MOF, Zn-Cu-MOF-74-alloyed was prepared by mechanical amorphization and then aging of the 1:1 mixture of monometallic Zn-MOF-74 and Cu-MOF-74 in methanol vapors. All products are highly crystalline, with similar PXRD diffractograms (Figures S2-S5), Fourier transform infrared (FTIR) spectra (Figures S10-S13), and the molar ratio of two metals in bulk sample observed using flame atomic absorption spectroscopy (AAS). However, they show significant differences in their electron spin resonance (ESR) spectra and static magnetization properties. ^{13}C magic angle spinning nuclear magnetic resonance (^{13}C MAS NMR) spectra, together with the scanning electron microscopy with energy-dispersive X-ray spectroscopy (EDAX/SEM) and in-situ synchrotron PXRD monitoring[41,42] of the mechanochemical formation of MOFs were used for estimating the local ordering of the metal nodes in the chains and the rationalization of differences in magnetic properties of the three materials.

RESULTS

In order to determine the magnetic properties of the monometallic Cu-MOF-74, and to see how copper dilution with zinc and distribution within the framework affect magnetic properties of multivariate MOF-74 materials, initially we prepared Cu-MOF-74 by an adapted, recently described procedure.[30] Next, we prepared three multivariate MOF-74 materials that differ in synthetic pathways. ZnCu-MOF-74 material was prepared in a step-wise manner following a previously described procedure.[29] In the first step ZnO and H_4dobdc were milled together to form Zn-intermediate (Zn-INT, CCDC code: ODIPOH)[17,18] followed by introducing copper hydroxide in the second step, where the MOF-74 framework assembles upon further milling. Mechanochemical synthesis of CuZn-MOF-74 material was designed in an analogous way, preparing the Cu-INT in the first step and adding ZnO in the second step, resulting in crystalline CuZn-MOF-74 material. For the preparation of Zn-Cu-MOF-74-alloyed, a 1:1 mixture of crystalline Zn-MOF-74 and Cu-MOF-74 was milled, then dried and amorphized according to a recently described procedure.[30] The crystalline Zn-Cu-MOF-74-alloyed phase was obtained by aging of the amorphous mixture in methanol vapors. The details of the synthesis can be found in Section 1.1 in ESI. The different prepared phases of three MM-MOF-74 are indistinguishable by PXRD (Figure 2a) and their FTIR spectra closely resemble (Figure 2b). In the spectra of MOF-74 materials free carboxyl group stretching band of H_4dobdc ligand around 1640 cm^{-1} disappeared, and was replaced by bands around 1550 cm^{-1} and 1366 cm^{-1}, which correspond to the asymmetric and symmetric stretching of the coordinated carboxyl group, while the phenolic group stretching band shifted to 1246 cm^{-1}.[43] Certain amount of methanol remaining in the pores is manifested by a band at about 1025 cm^{-1}.[44] Molar ratio of the two metals in MM-MOF-74 materials is approximately 1:1, established on the basis of flame AAS and EDAX/SEM (Table S2).

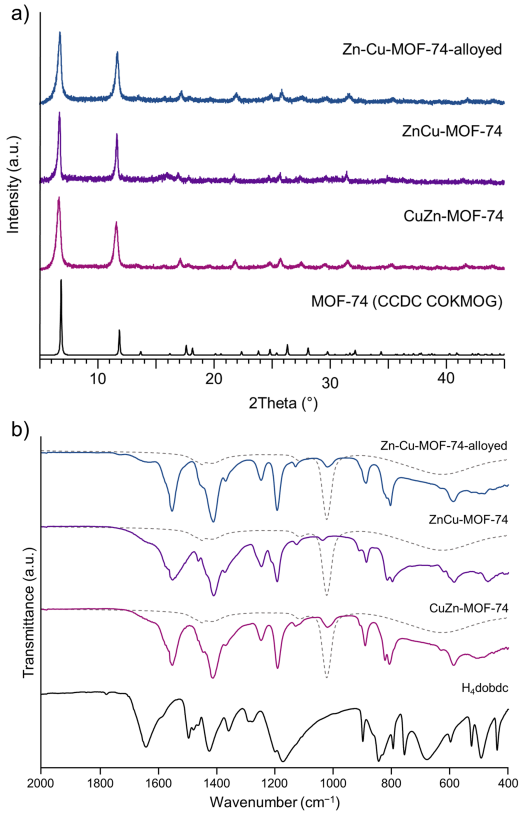

Figure 2. a) PXRD patterns of mechanochemically synthesized bimetallic copper/zinc MOF-74 materials (CuK_α radiation) compared to the simulated pattern of MOF-74 (CCDC code: COKMOG);[18,21] b) FTIR spectra of mechanochemically synthesized bimetallic copper/zinc MOF-74 materials compared to ligand H_4dobdc. Additional bands in the spectra are from residual MeOH (dashed line).

While the Zn-INT used in the preparation of ZnCu-MOF-74 was previously reported,[17,18] the Cu-INT detected in the first step of the two-step synthesis of CuZn-MOF-74 did not correspond to any known copper-H_4dobdc complex.[18] All attempts of solution synthesis and single crystal preparation of Cu-INT were unsuccessful due to its partial transformation into Cu-MOF-74 (Figure S1). The crystal structure of Cu-INT was therefore determined from room temperature PXRD data (Table S1), with the composition Cu(dobdc)$(H_2O)_2$ obtained through TGA analysis (Figures S7 and S8). The Cu-INT structure consists of square-pyramidally coordinated copper atoms, with two water molecules and two different dobdc molecules occupying the equatorial positions in a trans conformation, and a third dobdc molecule coordinated in the axial position (Figures 1c

and S9a). Importantly, each dobdc molecule bridges three different copper centers, two through each carboxylic group (non-chelating, equatorial binding of Cu), and one through one of the hydroxyl groups (axial position of Cu). This is markedly distinct from both the other previously reported $Cu(dobdc)(H_2O)_2$ compound (CCDC code: KUSNAQ),[18] and Zn-INT, where the hydroxyl groups of dobdc are uncoordinated, and the ligand is bound in a quasi-tetrahedral coordination (Figures 1d and S9b). For the full description of the Cu-INT crystal structure and the details of structure solution see Section 2.2 in ESI.

MAGNETIC CHARACTERIZATION

Monometallic Cu-MOF-74 sample

ESR study The temperature dependence of the X-band ESR and HF-ESR spectra of Cu-MOF-74 are shown in Figures 3a and 3b, respectively. The frequency vs. resonance field dependence obtained in the HF-ESR measurements at $T = 4$ K is presented in the inset to Figure 3b together with characteristic HF-ESR spectra. The analysis of the spectral shape reveals that it is composed of two contributions, one corresponding to non-interacting, purely paramagnetic, and other magnetically coupled spin species. With this assumption, the X-band spectrum at 10 K was successfully simulated by using the EasySpin software,[45] assuming spin-Hamiltonian with Zeeman and hyperfine terms:

$$\mathbf{H} = \mu_B \mathbf{B} \cdot \mathbf{g} \cdot \mathbf{S} + \mathbf{S} \cdot \mathbf{A} \cdot \mathbf{I}. \quad (1)$$

Here, $\mathbf{B}$ is the applied magnetic field, $\mathbf{g}$ is the g-tensor, $\mathbf{S}$ is the electron spin operator for copper spin ($S = 1/2$), μ_B is Bohr magneton, $\mathbf{A}$ is the hyperfine tensor and $\mathbf{I}$ is the nuclear spin operator for copper ($I = 3/2$). Both copper species in Cu-MOF-74 can be simulated with the same spin-Hamiltonian parameters: $\mathbf{g}$=[2.07 2.36] and $\mathbf{A}$=[0 400] MHz but with different line-widths of assumed Lorentzian lines, one broader and one narrower, for coupled and paramagnetic species, respectively. The used parameters of the simulation are given in Table S3 while the simulated spectrum at 10 K is presented in Figure 3a.

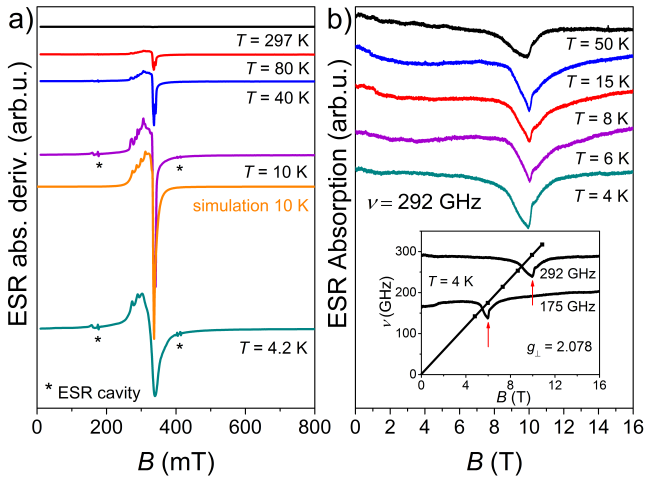

Figure 3. Temperature dependence of a) the X-band ESR spectra of the Cu-MOF-74 complex together with the simulated spectrum at 10 K, and b) the HF-ESR spectra of this complex. The frequency vs. resonance field diagram at 4 K for prominent points labeled by red arrows is shown in the inset to b) together with exemplary HF-ESR spectra. Asterisks in panel a) mark parasitic signals from the ESR cavity.

Magnetization study The field dependence of the magnetization $M(H)$ of Cu-MOF-74 at the lowest measured temperature of 1.8 K is shown in Figure 4a. Even at the highest applied field of 7 T, $M(H)$ is far from the expected saturation value $M_{sat} = ng\mu_B S$ (n is the number of magnetic moments per mole)[46] indicating a significant AFM interaction between the Cu spins in Cu-MOF-74. Namely, for one Cu(II) ion in a formula unit with $g = 2.171$ taken as the powder averaged g-factor $< g >= \sqrt{1/3(g_\parallel^2 + 2g_\perp^2)}$ from ESR results, M_{sat} should amount to 1.086 μ_B while a much smaller value of 0.12 μ_B is observed.

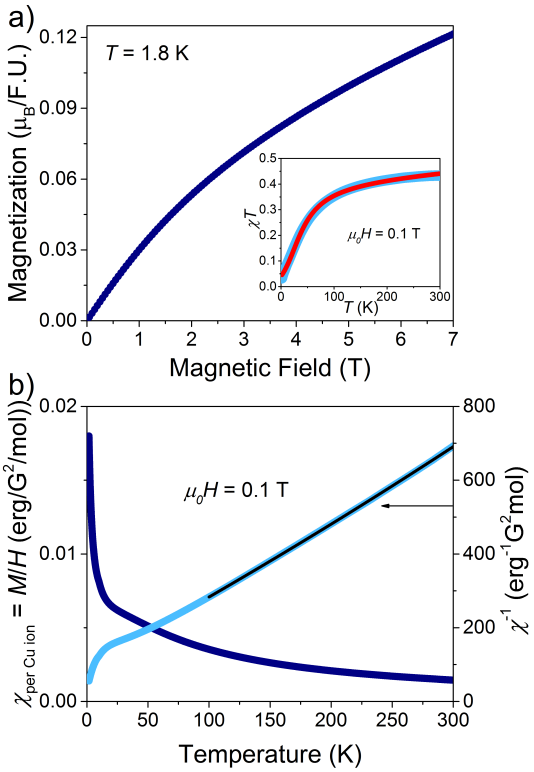

Figure 4. a) Field dependence of the magnetization $M(H)$ of Cu-MOF-74 at $T = 1.8$ K. The inset shows the temperature dependence of the product $\chi(T)T$ in units of erg K/(G^2 mol). Red solid line represents the fit to the extended Bonner-Fisher model for $S = 1/2$ according to Eqs. S1 and S2. b) Temperature dependence of the magnetic susceptibility $\chi(T)$ of Cu-MOF-74 and of its inverse $\chi^{-1}(T)$ measured in a field of 0.1 T. The black solid line is the fit to the Curie-Weiss law given by Eq. 2. The fitting results are presented in Table 1.

This conclusion is corroborated on the quantitative level by the analysis of the temperature dependence of the magnetic susceptibility $\chi(T)$ presented in Figure 4b. Fitting of the $\chi(T)$ curve (in the range 100–300 K) with the Curie-Weiss law[47]

$$\chi = C/(T - \Theta), \quad (2)$$

yields the Weiss temperature $\Theta \approx -55$ K and the Curie constant $C \approx 0.57$ erg K/(G^2 mol) (Table 1). This value of C is somewhat larger than the expected Curie constant of the non-interacting Cu spins $C = (n\mu_B^2 g^2 S(S+1))/(3k_B) = 0.442$ erg K/(G^2 mol), where k_B is the Boltzmann constant.[46] Such an overestimate may be related to a large value of Θ comparable to the temperatures of the fitting range while, strictly speaking, Eq. 2 is applicable at $T \gg \Theta$, only. Indeed, the product $\chi(T)T$ plotted in the inset to Figure 4a is very small at low temperatures as expected for the strong AFM coupling and gradually increases to its temperature independent limit $\chi(T)T \approx C$ by approaching room tempera-

ture where it gives a more realistic estimate of $C \approx 0.433$ erg K/(G^2 mol).

Considering the chain structure of Cu-MOF-74 and the AFM type of the $M(H)$ and $\chi(T)$ dependences, the $\chi T(T)$ curve was fitted in the entire temperature range to the AFM spin-chain Bonner-Fisher model, including also the inter-chain mean field correction Eqs. S1, S2 and S3.[48,49]

The fit result plotted as the red solid line in Figure 4a-inset yielded the nearest neighbor intra-chain AFM exchange constant $J \approx -57$ K and the residual inter-chain coupling $j \approx 7.5$ K. Also, the fit requires adding a Curie term C/T to account for paramagnetic Cu ions around 9%. Such a significant amount of the 'paramagnetic' Cu sites may originate from the boundaries of the nanometer-sized crystallites usual for mechanochemical synthesis, and is in agreement with the value of 10% obtained from ESR simulations (Table S3).

Bimetallic Cu/Zn-MOF-74 samples

ESR study Experimental X-band ESR spectra of CuZn-MOF-74, ZnCu-MOF-74 and Zn-Cu-MOF-74-alloyed at different temperatures are shown in Figure 5a together with their simulations at $T = 10$ K made on the basis of the spin-Hamiltonian (Eq. 1) and under the assumption of the presence of a two-component spin system in these materials, similar to the analysis in the previous section. The spin-Hamiltonian parameters g =[2.07 2.36] and A=[0 400] MHz appeared to be the same as those used for the simulation of the Cu-MOF-74 ESR spectra, but with the different weights of the spectral components, linewidths and g-strain values (Table S3).

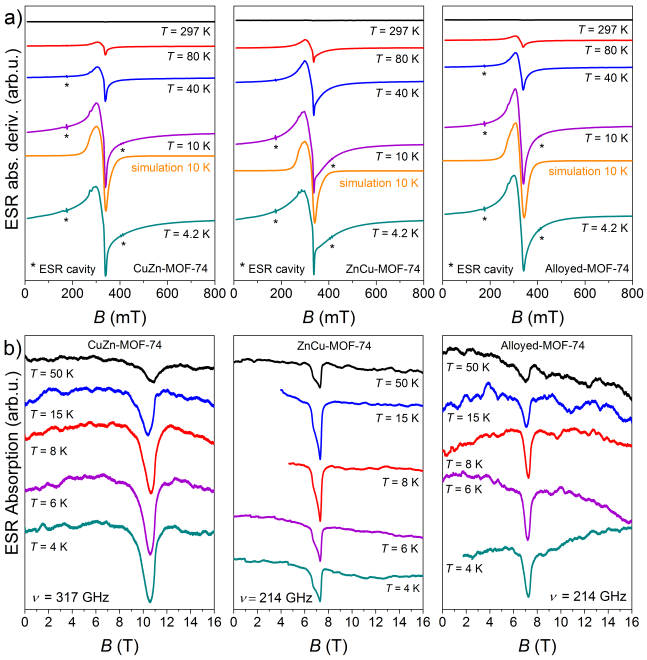

Figure 5. Temperature dependence of the ESR spectra of CuZn-MOF-74, ZnCu-MOF-74 and Zn-Cu-MOF-74-alloyed complexes. a) The X-band spectra together with the simulated spectra at 10 K. b) The HF-ESR spectra. Asterisks in panel a) mark parasitic signals from the ESR cavity.

The temperature dependence of the HF-ESR spectra of the investigated MOF samples is presented in Figure 5b. Lowering the temperature results in an increase of the spectral intensity, as expected, while the shape of the lines, their widths and the position do not change. The HF-ESR spectrum of ZnCu-MOF-74 exhibits a typical powder pattern with a peak and a shoulder corresponding to $g_\perp$ and $g_\parallel$, respectively. In contrast, the spectra of CuZn-MOF-74 and Zn-Cu-MOF-74-alloyed are single Lorentzian-shaped lines pointing at the presence of significant AFM interactions in these compounds resulting in a well-known exchange narrowing effect.[50,51] These observations are in agreement with the magnetic susceptibility data (see below) and obtained Weiss parameters given in Table 1. The more narrow line of Zn-Cu-MOF-74-alloyed indicates a stronger AFM interaction as compared to CuZn-MOF-74. The frequency dependence of the HF-ESR spectra of the mixed-metals MOFs was recorded at $T = 4$ K at several chosen frequencies from 142 to 317 GHz. The frequency vs. resonant magnetic field diagram, together with the selected spectra, are shown in Figure S17 of ESI. From this dependence the approximate values of the g-factors were determined and their values are presented in the insets of the respective graphs.[52–54]

Magnetization study The field dependence of the magnetization $M(H)$ of CuZn-MOF-74, ZnCu-MOF-74 and Zn-Cu-MOF-74-alloyed recorded at 1.8 K are shown in Figure 6a. The $M(H)$ curve of Cu-MOF-74, discussed in the previous section, is plotted in the same graph for comparison. One can notice that all three $M(H)$-curves of the mixed compounds are mutually different and also are very different from that of Cu-MOF-74. At the maximum magnetic field of 7 T, the magnetization is far from the saturation for all compounds pointing at the presence of significant AFM interactions in these materials.

It is interesting to note that the magnetization is lowest for the Cu-MOF-74 sample although it has two times more copper ions per formula unit as compared to mixed samples. This is, in fact, expected since in Cu-MOF-74 the majority of the Cu ions are coupled into AFM spin-chains and only a small fraction remains 'free' giving rise to the paramagnetic Curie contribution to the sample's magnetization and susceptibility at low temperatures. The nonmagnetic dilution in the mixed MOF-74 systems increases the amount of paramagnetic spins as compared to the monometallic version and yields larger magnetization. If the Cu and Zn ions in a 1:1 proportion would randomly occupy the metal sites in the structure, all three $M(H)$ curves should overlap. It is clear from Figure 6a that this is not the case. Obviously, a random distribution is not achieved in the mixed samples and, depending on the synthetic route, various types of spin clustering may take place, which is also reflected in a distinct behavior of the magnetic susceptibility $\chi(T)$.

The temperature dependence of $\chi(T)$ and of the product $\chi(T)T$ for all three mixed samples are presented in Figures 6b and 6c, along with the respective curves for the monometallic Cu-MOF-74 sample, scaled by a factor of 0.5 to account for the presence of two copper ions in the formula unit. The high temperature part (50–300 K) of the $\chi(T)$ dependence can be fitted to the Curie-Weiss law (Eq. 2), as shown in the inset to Figure 6c, with the parameters listed in Table 1. The weakening of the average AFM interactions due to nonmagnetic dilution is reflected in the reduction of the Weiss temperature Θ. Still, the numbers obtained should be considered only as an order of magnitude estimate due to the complexity of the spin structures in the mixed compounds, as discussed below.

At room temperature the product χT for the mixed ZnCu-MOF-74 and Zn-Cu-MOF-74-alloyed complexes exceeds the ideal value $\chi(T)T \approx C = 0.442$ erg K/(G^2 mol) expected

Table 1. Parameters of the fit to the Curie-Weiss law Eq. 2, to the extended Bonner-Fisher model Eqs. S1, S2 and S3, and to the Bleaney-Bowers dimer model Eqs. S4 and S5. For details, see the main text and ESI.

Sample	Temp. range Curie-Weiss	C (erg K/(G^{2}mol))	Θ (K)	J/k_B (K)	j/k_B (K)	Paramag. species %
Cu-MOF-74	100–300 K	0.5710(5)	-54.5(1)	-56.8(2)	7.5(3)	9.06(5)
CuZn-MOF-74	50–300 K	0.5150(3)	-18.70(5)	-36.0(3)	13.3(4)	33.5(1)
ZnCu-MOF-74	50–300 K	0.5050(2)	-1.81(3)	-11.19(1)		37.59(4)
Zn-Cu-MOF-74-alloyed	50–300 K	0.4660(1)	-19.51(1)			

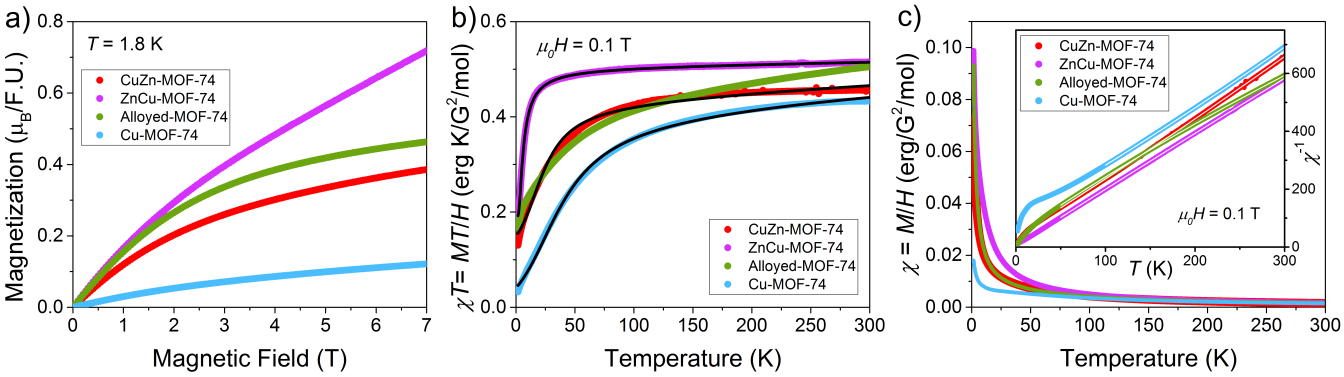

Figure 6. a) Field dependence of the magnetization $M(H)$ of the mixed CuZn-MOF-74, ZnCu-MOF-74 and Zn-Cu-MOF-74-alloyed samples and of the monometallic Cu-MOF-74 at $T = 1.8$ K. b) Temperature dependence of the magnetic susceptibility $\chi(T)$ multiplied by T measured in a field of 0.1 T for the same samples. Black solid lines represent the fit to the extended Bonner-Fisher model for Cu-MOF-74 and CuZn-MOF-74 samples, and the Bleaney-Bowers model for the ZnCu-MOF-74 sample. c) Temperature dependence of $\chi(T)$ (main panel) and of its inverse $\chi^{-1}(T)$ of the same samples in a field of 0.1 T. White solid lines in the inset are the fits to the Curie-Weiss law according to Eq. 2.

for an equal amount of the Cu and Zn ions suggesting slight excess of the magnetic Cu ions in these samples. As the EDAX-SEM and AAS analyses (Table S2) both show almost identical metal composition in all samples, this difference likely stems from the unequal composition of the guests in pores of these molecular sponges, where the water and methanol may exchange thus slightly changing the molar mass of materials and influencing the absolute values of magnetic susceptibility.

As discussed in the previous section, a strong reduction of the product $\chi(T)T$ at low temperatures for the monometallic Cu-MOF-74 sample is due to a significant AFM interaction between the majority of the Cu ions arranged into the spin-chains whereas noninteracting, paramagnetic Cu ions are present in a relatively small amount of 9–10% only. An appreciable increase of $\chi(T)T$ at low T for the mixed samples indicates fragmentation of the AFM spin-chains into shorter segments and a corresponding increase of the concentration of uncompensated spins up to 30–40%, in agreement with the values obtained from ESR simulations $\sim 30\%$ (Table S3).

Theoretical models In addition to the standard Curie-Weiss model used, by comparing the shapes of the $\chi(T)T$ curves it is possible to derive some qualitative conclusions on the feasible spin arrangements in the mixed compounds. The $\chi(T)T$ dependence for CuZn-MOF-74 is most similar to that for Cu-MOF-74. This suggests that in the synthetic route of CuZn-MOF-74 first the Cu ions form the AFM spin-chains which then Zn ions break into the segments of different length. Conversely, it seems that in ZnCu-MOF-74 first the nonmagnetic Zn chains are formed and then Cu ions break their continuity yielding spin monomers (paramagnetic centers), spin dimers or some short spin-chain segments.

In view of the various types of the Cu/Zn site disorder present in the mixed CuZn-MOF-74 and ZnCu-MOF-74 complexes it is not feasible to define a unique microscopic spin interaction model which would enable a unified fitting of the measured susceptibility curves of these compounds. The magnetic behavior of the CuZn-MOF-74 complex is qualitatively closest to its monometallic counterpart Cu-MOF-74 suggesting applicability of the extended AFM spin-chain Bonner-Fisher model to CuZn-MOF-74 (Eqs. S1, S2 and S3). Indeed, its $\chi(T)T$ dependence can be reasonably well fitted to this model yielding the intra-chain exchange constant $J \approx -36$ K and the positive inter-chain exchange constant $j \approx 13$ K (Figure 6b). This result shows that the AFM interaction within the chain segments is weakened in comparison to Cu-MOF-74, and there is an appreciable effective FM interaction between these segments.

The $\chi T(T)$ curve for ZnCu-MOF-74 is more reminiscent of that for spin dimers and, in fact, the Bleaney-Bowers AFM dimer model (Eqs. S4 and S5) nicely reproduces the experimental dependence with the intra-dimer exchange constant $J \approx -11$ K (Figure 6b).[49,55] Nevertheless, the presence of more extended spin clusters, e.g., trimers and tetramers, in this compound cannot be excluded.

The alloyed compound shows a completely different magnetic behavior as compared with both ZnCu- and CuZn-MOF-74. Presumably, the Cu-based spin system of this compound is composed of spin-chain fragments with a distribution of the superexchange interaction strengths and therefore reasonable physical model here could not be performed. An indication for that is a continuous increase of the product $\chi(T)T$ even above the room temperature despite a rather small value of Θ derived from the Curie-Weiss fit (Table 1). This behaviour above 100 K is very similar to the behaviour of Cu-MOF-74 curve, but disagreement between these two curves could be seen in the low-temperature region, due to different magnetic compositions.

SOLID-STATE NMR

Solid-state NMR spectroscopy can often provide additional insight into the local structure of solids, therefore ^{13}C MAS NMR spectra of CuZn-MOF-74, ZnCuMOF-74 and Zn-Cu-MOF-74-alloyed were recorded and compared to the spectra of pure crystalline Cu-MOF-74 and Zn-MOF-74 (Figure 7). The spectra of CuZn-MOF-74 and ZnCuMOF-74 are very similar one to another. They both show a high, sharp signal of methanol molecules at about 50 ppm, and a large number of broad signals with isotropic shifts ranging from about -100 ppm to 700 ppm. Large positive and negative isotropic shifts are typical for carbon nuclei in close proximity to paramagnetic centers. The fact that the signals do not appear only at shifts characteristic for either Cu-MOF-74 or Zn-MOF-74 suggests that carbon nuclei within these two samples experience many different environments – most probably because the dobdc linkers of the MOF-74 framework connect not only metal nodes of a single type but also metal nodes of two different types (i.e. dobdc linkers can be bound to various numbers of Cu and Zn centers). In other words, the large number of signals and the spread of their isotropic chemical shifts suggests that in CuZn-MOF-74 and ZnCuMOF-74 copper and zinc atoms are mixed within the frameworks on the (sub)nanometer scale.

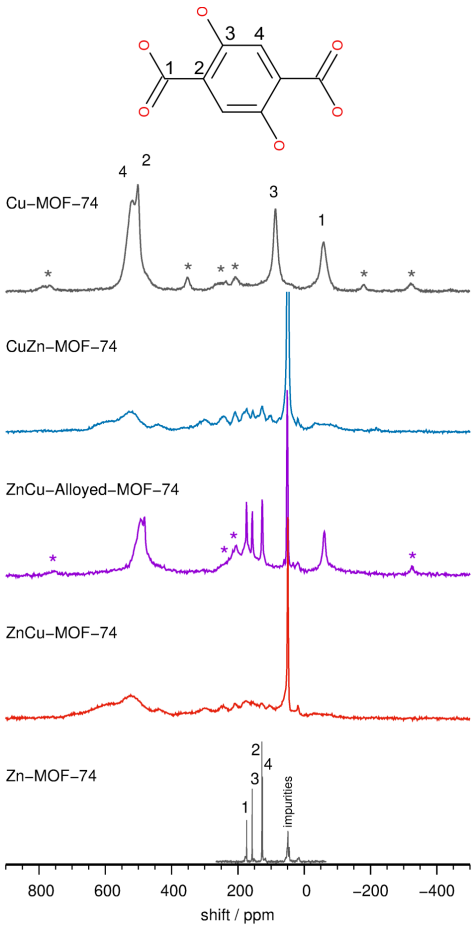

Figure 7. ^{13}C MAS NMR spectra of mixed-metal CuZn-MOF-74, ZnCu-MOF-74, and Zn-Cu-MOF-74-alloyed compared to the spectra of neat Cu-MOF-74 and Zn-MOF-74. Assignment of the carbon NMR signals of Zn-MOF-74 is based on the solution spectrum of H_2dobdc, whereas the assignment of the carbon NMR signals of Cu-MOF-74 is based on ^{13}C spin-lattice relaxation measurements and DFT-based calculations of hyperfine coupling constants.[56] Asterisks denote spinning sidebands.

The ^{13}C MAS NMR spectrum of Zn-Cu-MOF-74-alloyed is different from the spectra of the above described mixed-metal samples and strongly suggests that the alloyed sample is a physical mixture of Cu-MOF-74 and Zn-MOF-74 particles or is built of large copper-based and zinc-based domains. In the spectrum of Zn-Cu-MOF-74-alloyed we can see strong sharp signals at 174, 157, 128 and 126 ppm, which are typical for neat Zn-MOF-74, and broad signals at about 500 and -60 ppm, which very much resemble the signals of neat Cu-MOF-74. The signal of the C3 carbon nuclei, which can be found at 90 ppm in the spectrum of neat Cu-MOF-74, is shifted in the spectrum of the alloyed sample and overlaps with a sharp signal of the zinc-based particles and the spinning sidebands of the signals of the copper-based particles in the range between 170 ppm and 210 ppm. Taking into account that Zn-Cu-MOF-74-alloyed contains a large amount of methanol molecules or methohxy species, such a shift is not surprising - even subtle changes of the local environment of copper centers can lead to notable changes in the magnitude of the hyperfine coupling between the unpaired electrons of Cu(II) and the ^{13}C nuclei and thus in the isotropic shift of these nuclei.

EDAX/SEM ANALYSIS

Elemental maps obtained by EDAX/SEM analysis indicate homogenous distribution of Cu and Zn throughout the selected areas of the CuZn-MOF-74 and ZnCu-MOF-74 samples, respectively (Figures S14 and S15) with Cu/Zn molar ratios of approximately 0.95 in both cases (Table S2). On the other hand, in spite of slightly lower Zn content (Cu/Zn = 1.03), the agglomerates of Zn-Cu-MOF-74-alloyed sample contain some Zn-rich domains/grains implying lower homogeneity of the distributed metal cations (Figure S16). These results are in line with the metal ratios determined in bulk samples using flame AAS.

REAL-TIME IN-SITU MONITORED SYNTHESES

To gain insight into the mechanism of mechanochemical synthesis of copper/zinc MOF-74 materials and to rationalize the observed differences in the magnetic properties of these materials, as well as the differences compared to monometallic Cu-MOF-74, we designed several real-time in-situ PXRD monitoring experiments and carried them out at the Deutsches Elektronen-Synchroton (DESY), described in ESI. For in-situ PXRD monitoring experiments, pre-prepared intermediates Zn-INT and Cu-INT were used, to both closely mimic the two-step synthetic route, but also simplify the studied system.

ZnCu-MOF-74 In-situ PXRD monitoring of the synthesis of ZnCu-MOF-74 was performed by milling Zn-INT and Cu(OH)2 in a 1:1 stoichiometric ratio with the addition of a small amount of MeOH. Intensities of the reflections of the reactants decrease within the first few minutes of milling. The reflections of MOF-74 appear 6 minutes from the onset of milling, along with those of UTSA-74,[57] a recently discovered high-temperature MOF-74 polymorph. This phase forms jointly with the MOF-74 phase and transforms to pure ZnCu-MOF-74 after an additional 10 minutes of milling (Figure 8a).

CuZn-MOF-74 Next, CuZn-MOF-74 was prepared by milling Cu-INT and ZnO in a 1:1 stoichiometric ratio, with the addition of a small amount of MeOH. Within 5 min from the start of milling, the reflections of MOF-74 start to

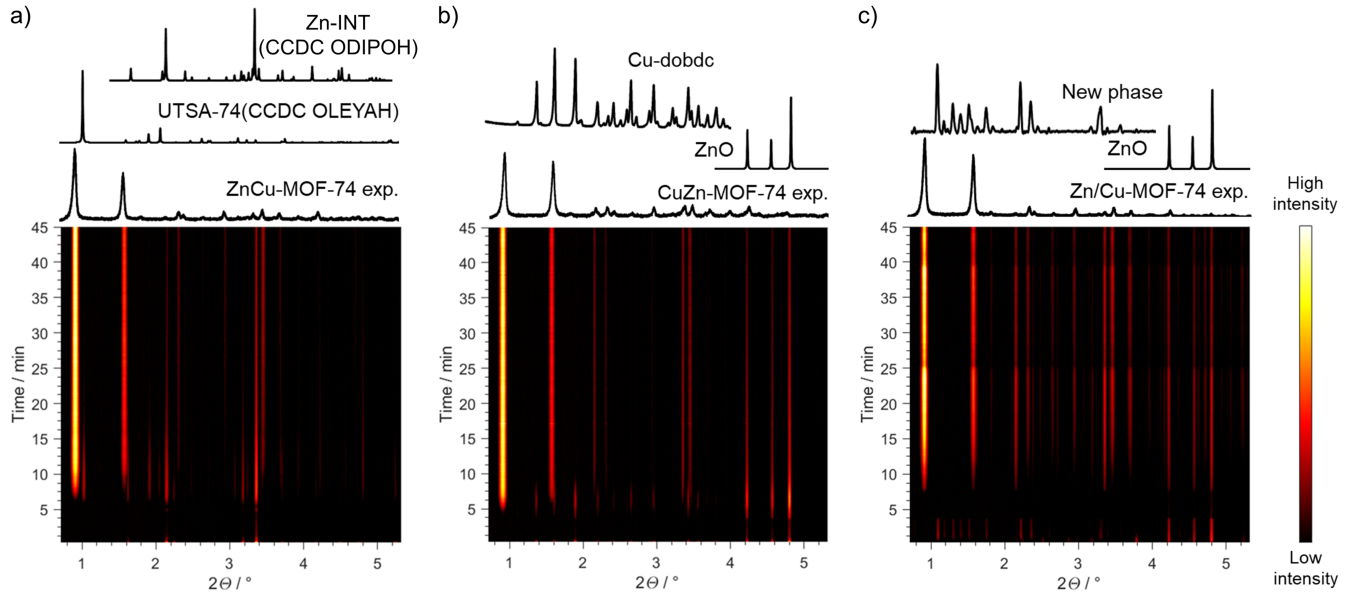

Figure 8. a) Time-resolved diffractograms from the in situ and real-time monitoring of the synthesis of ZnCu-MOF-74 from $[Zn(H_2dobdc)(H_2O)_2]$ and $Cu(OH)_2$ by LAG (MeOH). b) Time-resolved diffractograms for the synthesis of CuZn-MOF-74 from $[Cu(H_2dobdc)(H_2O)_2]$ and ZnO by LAG (MeOH). c) Time-resolved diffractograms for the synthesis of Zn/Cu-MOF-74 from ZnO, $Cu(OH)_2$ and H_4dobdc by LAG (H_2O, MeOH). Diffraction patterns of observed crystalline phases are given on the top. X-ray beam: $E \approx 60$ keV, $\lambda = 0.20735$ Å.

appear, and after 10 minutes the peaks of Cu-INT disappear completely (Figure 8b). Unlike Cu-INT, the consumption of ZnO is gradual and slower, and the reflections of ZnO are detectable for further 15 minutes milling (Figure S18).

Zn/Cu-MOF-74-one-step To establish the reactivity and affinity of the two metal sources for the binding to H_4dobdc, we explored the mechanochemical formation of zinc/copper MOF-74 by performing the milling of ZnO, $Cu(OH)_2$ and H_4dobdc in a 1:1:1 stoichiometric ratio with the addition of small amounts of H_2O and MeOH. During the first minute of the synthesis a new phase is detected. MOF-74 reflections are observed after 8 minutes milling, and after 25 minutes MOF-74 is the only observable crystalline phase (Figure 8c). We identified the unknown phase to be a mixture of three copper H_2dobdc complexes: cis-$[Cu(H_2dobdc)(H_2O)_2]$ (CCDC code: KUSNAQ),[18] trans-$[Cu(H_2dobdc)(H_2O)_2]$ (Cu-INT, identified in this study) and a copper complex with H_2dobdc (of yet unknown structure) that can be prepared by milling $Cu(OH)_2$ and H_4dobdc in a 1:1 stoichiometric ratio using excess MeOH as a liquid additive (Figure S19).

DISCUSSION

Mechanochemical procedures are now well known for their high level of stoichiometric control and the ability to open pathways towards unique products, as was also the case with the bimetallic MOF-74 materials.[29] In situ PXRD monitoring shows that the Zn-INT to ZnCu-MOF-74 transformation occurs as multi-step process trough transient UTSA-74 phase[57] (Figure 8a). The reaction goes without any observable transformation of Zn-INT to Cu-INT phase, indicating that the copper did not exchange the zinc from the carboxylate sites. Together with the results of solid-state NMR and magnetic studies one can assume that this process includes the incorporation of copper atoms at available free metal sites, leading to a homogeneous distribution of copper nodes in the oxo-chains of the MOF and the most paramagnetic-like behavior in comparison with remaining two materials.

The slower consumption of ZnO in the formation of CuZn-MOF-74 from the Cu-INT, compared to the MOF-74 formation (Figures 8b and S18) is indicative of process where the copper(II) nodes from the Cu-INT partially react into the Cu-MOF-74, same as was already observed during the crystallization of Cu-INT in methanol, unlike the zinc analogue. The higher reactivity of the Cu(II) for the dobdc ligand is corroborated by the monitoring of the formation of copper/zinc MOF-74 from the mixture of ZnO and $Cu(OH)_2$, where different copper intermediate phases are formed (Figures 8c and S19). The different reactivity and affinity of two metals for the dobdc ligand, and the unique structure of the Cu-INT, where even the less reactive phenolic groups coordinate the copper node, may explain also the differences between the different structures of the oxometallic chains and magnetic properties of the three tested copper/zinc MOFs. The higher reactivity of copper, even for phenolic groups, will induce the formation of longer chains containing exclusively the copper nodes for the CuZn-MOF-74. The efficient dispersion of copper nodes in the ZnCu-MOF-74 results in higher magnetization than Cu-MOF-74, despite ZnCu-MOF-74 containing half the copper(II) nodes. It reveals that the copper is not exchanging the zinc node coordinated to carboxylate. It rather coordinates the remaining phenolic groups, leading to the observed magnetic properties of the ZnCu-MOF-74.

Another exciting observation is the short occurrence of the fleeting UTSA-74 polymorph, which is most likely a mixed-metal phase. UTSA-74 emerged only in a few instances until now, showing new and exciting properties to MOF-74. The possibility to form the mixed-metal UTSA-74 may expand the application potential for these two MOF polymorphs.

CONCLUSION

Here presented magnetic analysis shows that magnetically active nodes can be efficiently dispersed in the bimetallic copper/zinc-MOF-74 material, leading to the different magnetic properties as compared to the monometallic Cu-MOF-74. Cu-MOF-74 can be described, using the extended Bonner-Fisher model, as antiferromagnetic copper chains ($J \approx -57\ K$) with weaker inter-chain ferromagnetic interaction ($j \approx 7.5\ K$). This is an interesting result as all the other known magnetic MOFs-74, Co-MOF-74, Fe-MOF-74 and Ni-MOF-74, containing nodes with spin higher than 1/2, have ferromagnetically coupled metal ions inside the oxo-chains while the inter-chain interactions are antiferromagnetic.[20,32,37,38] Small changes in spin states and magnetic anisotropy, as well as subtle structural changes, led to substantially different magnetic behaviors. Combined with the open coordination sites on the metal nodes present in the 1D oxometallic chains, this makes MOF-74 family a particularly interesting platform for the investigation of low-dimensional magnetism in MOFs.

Although mixed-metal MOFs have almost indistinguishable PXRD and FTIR, different magnetic behaviors reveal different interactivity of copper(II) and zinc(II) ions inside MOF structures. CuZn-MOF-74, obtained via the new complex Cu-INT, can be described as a combination of isolated paramagnetic copper species and longer copper-copper associations; CuZn-MOF-74 can be described similarly as monometallic Cu-MOF-74 using extended Bonner-Fisher model but with reduced strength of intra-chain coupling ($J \approx -36$ K) with FM inter-chain interaction ($j \approx 13\ K$). On the other hand, ZnCu-MOF-74, obtained via Zn-INT complex, can be described as a combination of well isolated paramagnetic copper species and short copper dimers fitted by the Bleaney-Bowers model ($J \approx -11$ K). According to magnetic, EDAX/SEM, and SS NMR results, the alloyed sample seemed to be predominantly a physical mixture of Cu-MOF-74 and Zn-MOF-74 domains, with mixed phases on the grain interfaces. Our results also show that the application of MOFs as real system magnets will be in part complicated with the hard-to-control content of the pores. The dynamic exchange of the solvent in pores with the atmosphere will influence the absolute magnetization values due to the change of the molar mass of the compound.

Performing real-time in-situ synchrotron PXRD monitored synthesis, the obtained difference is rationalized with different copper vs. zinc reactivity and the affinity of the copper or zinc towards the functional groups of the ligand. While the mechanochemical procedure offers yet the unprecedented level of control in the synthesis of bimetallic MOFs from monometallic coordination polymers, the synthetic process still relies on the nature and affinity of the chemical species at hand. The experimentalist must take into account, in the future design and production of bimetallic MOF-74 materials, parameters such as the structure of the coordination polymer reactant and the reactivity of the metal nodes for the particular binding group on the ligand, but also the order in which the two metals are added into the reaction. In the presented case, zinc is strongly bound in Zn-INT, resulting in an efficient dispersion and isolation of paramagnetic copper nodes added in the second synthetic step. On the other hand, the high reactivity of Cu(II) for H_4dobdc leads to the formation of directly bound longer copper chain-clusters in the formed material and different magnetic properties.

We will now focus on determining magnetic properties for new bimetallic MOF-74 materials containing pairs of paramagnetic centers such as Co(II), Mn(II), Fe(II), Ni(II), and Cu(II) to explore the magnetic properties in these materials stemming from close contacts and interactions between centers with different spin states. We also aim to tune the synthetic parameters towards the stabilization of bimetallic UTSA-74 polymorph, which would present a particularly interesting class of magnetic compounds.

Acknowledgement We thank the Croatian Science Foundation (IP-2018-01-3168 and UIP-2014-09-9775) and DAAD-MZO bilateral project: *Magneto-structural correlations in molecular magnetic complexes studied by electron spin resonance spectroscopy* for financial support. The work has been supported by the "Research Cooperability" Program of the Croatian Science Foundation funded by the EU from the European Social Fund under the Operational Programme Efficient Human Resources 2014-2020, through grant PZS-2019-02-4129. Parts of this research were carried out at DESY PETRA III P02.1 beamline. The beamtime was allocated by an in-house contingent. D.P. acknowledges the support of project CeNIKS cofinanced by the Croatian Government and the EU through the European Regional Development Fund: Competitiveness and Cohesion Operational Programme (Grant KK.01.1.1.02.0013). M.M. and G.M. acknowledge the financial support from the Slovenian Research Agency (research core funding No. P1-0021 and project No. N1-0079). I.B. acknowledges support from the Polish National Agency for Academic Exchange (Ulam Scholarship PPN/ULM/2020/1/00216). M.A. acknowledges support from Narodowe Centrum Nauki (NCN, Poland), grant no. 2018/31/D/ST5/03619.

References

(1) Li, H.; Eddaoudi, M.; O'Keeffe, M.; Yaghi, O. M. Design and synthesis of an exceptionally stable and highly porous metal–organic framework. *Nature* **1999**, 276–279.

(2) Rosi, N. L.; Kim, J.; Eddaoudi, M.; Chen, B.; O'Keeffe, M.; Yaghi, O. M. Rod Packings and Metal–Organic Frameworks Constructed from Rod-Shaped Secondary Building Units. *J. Am. Chem. Soc.* **2005**, *127*, 1504–1518.

(3) Zhou, H.-C.; Long, J. R.; Yaghi, O. M. Introduction to Metal–Organic Frameworks. *Chem. Rev.* **2012**, *112*, 673–674.

(4) Minguez Espallargas, G.; Coronado, E. Magnetic functionalities in MOFs: from the framework to the pore. *Chem. Soc. Rev.* **2018**, *47*, 533–557.

(5) Thorarinsdottir, A. E.; Harris, T. D. Metal–Organic Framework Magnets. *Chem. Rev.* **2020**, *120*, 8716—8789.

(6) Abednatanzi, S.; Derakhshandeh, P. G.; Depauw, H.; Coudert, F.-X.; Vrielinck, H.; Van Der Voort, P.; Leus, K. Mixed-metal metal–organic frameworks. *Chem. Soc. Rev.* **2019**, *48*, 2535–2565.

(7) Masoomi, M. Y.; Morsali, A.; Dhakshinamoorthy, A.; Garcia, H. Mixed-Metal MOFs: Unique Opportunities in Metal–Organic Framework (MOF) Functionality and Design. *Angew. Chem. Int. Ed.* **2019**, *58*, 15188–15205.

(8) Viciano-Chumillas, M.; Liu, X.; Leyva-Pérez, A.; Armentano, D.; Ferrando-Soria, J.; Pardo, E. Mixed component metal-organic frameworks: Heterogeneity and complexity at the service of application performances. *Coord. Chem. Rev.* **2022**, *451*, 214273.

(9) Guo, W.; Xia, W.; Cai, K.; Wu, Y.; Qiu, B.; Liang, Z.; Qu, C.; Zou, R. Kinetic-Controlled Formation of Bimetallic Metal–Organic Framework Hybrid Structures. *Small* **2017**, *13*, 1702049.

(10) Kalaj, M.; Cohen, S. M. Postsynthetic Modification: An Enabling Technology for the Advancement of Metal–Organic Frameworks. *ACS Cent. Sci.* **2020**, *6*, 1046–1057.

(11) Santaclara, J. G.; Olivos-Suarez, A. I.; Gonzalez-Nelson, A.; Osadchii, D.; Nasalevich, M. A.; van der Veen, M. A.; Kapteijn, F.; Sheveleva, A. M.; Veber, S. L.; Fedin, M. V.; Murray, A. T.; Hendon, C. H.; Walsh, A.; Gascon, J. Revisiting the Incorporation of Ti(IV) in UiO-type Metal–Organic Frameworks: Metal Exchange versus Grafting and Their Implications on Photocatalysis. *Chem. Mater.* **2017**, *29*, 8963–8967.

(12) Garai, B.; Bon, V.; Krause, S.; Schwotzer, F.; Gerlach, M.; Senkovska, I.; Kaskel, S. Tunable Flexibility and Porosity of the Metal–Organic Framework DUT-49 through Postsynthetic Metal Exchange. *Chem. Mater.* **2020**, *32*, 889–896.

(13) Lalonde, M.; Bury, W.; Karagiaridi, O.; Brown, Z.; Hupp, J. T.; Farha, O. K. Transmetalation: routes to metal exchange within metal–organic frameworks. *J. Mater. Chem. A* **2013**, *1*, 5453–5468.

(14) Nouar, F.; Devic, T.; Chevreau, H.; Guillou, N.; Gibson, E.; Guillaume Clet, G.; Daturi, M.; Vimont, A.; Grenèche, J. M.; Breeze, M. I.; Walton, R. I.; Llewellyne, P. L.; Serre, C. Tuning the breathing behaviour of MIL-53 by cation mixing. *Chem. Commun.* **2012**, *48*, 10237–10239.

(15) Caskey, S. R.; Matzger, A. J. Selective Metal Substitution for the Preparation of Heterobimetallic Microporous Coordination Polymers. *Inorg. Chem.* **2008**, *47*, 7942–7944.

(16) Wang, Y.; Bredenkötter, B.; Rieger, B.; Volkmer, D. Two-dimensional metal–organic frameworks (MOFs) constructed from heterotrinuclear coordination units and 4,4'-biphenyldicarboxylate ligands. *Dalton Trans.* **2007**, 689–696.

(17) Ghermani, N. E.; Morgant, G.; d'Angelo, J.; Desmaële, D.; Fraisse, B.; Bonhomme, F.; Dichi, E.; Sgahier, M. Covalently bonded infinite zigzag chain structure in a novel Zn(II) complex of 2,5-dihydroxy-1,6-benzenedicarboxylic acid. *Polyhedron* **2007**, *26*, 2880–2884.

(18) Groom, C. R.; Bruno, I. J.; Lightfoot, M. P.; Ward, S. C. The Cambridge Structural Database. *Acta Crystallogr.* **2016**, *B72*, 171–179.

(19) Li, H.; Yang, Z.; Lu, S.; Su, L.; Wang, C.; Huang, J.; Zhou, J.; Tang, J.; Huang, M. Nano-porous bimetallic CuCo-MOF-74 with coordinatively unsaturated metal sites for peroxymonosulfate activation to eliminate organic pollutants: Performance and mechanism. *Chemosphere* **2021**, *273*, 129643.

(20) Dietzel, P. D. C.; Morita, Y.; Blom, R.; Fjellvåg, H. An In Situ High-Temperature Single-Crystal Investigation of a Dehydrated Metalic–Organic Framework Compound and Field-Induced Magnetization of One-Dimensional Metal–Oxygen Chains. *Angew. Chem. Int. Ed.* **2005**, *44*, 6354–6358.

(21) Queen, W. L. et al. Comprehensive study of carbon dioxide adsorption in the metal–organic frameworks M2(dobdc) (M = Mg, Mn, Fe, Co, Ni, Cu, Zn). *Chem. Sci.* **2014**, *5*, 4569–4581.

(22) Xiao, T.; Liu, D. The most advanced synthesis and a wide range of applications of MOF-74 and its derivatives. *Micropor. Mesopor. Mat.* **2019**, *283*, 88–103.

(23) Lee, K.; Howe, J. D.; Lin, L.-C.; Smit, B.; Neaton, J. B. Small-Molecule Adsorption in Open-Site Metal–Organic Frameworks: A Systematic Density Functional Theory Study for Rational Design. *Chem. Mater.* **2015**, *27*, 668–678.

(24) Sun, D.; Sun, F.; Deng, X.; Li, Z. Mixed-Metal Strategy on Metal–Organic Frameworks (MOFs) for Functionalities Expansion: Co Substitution Induces Aerobic Oxidation of Cyclohexene over Inactive Ni-MOF-74. *Inorg. Chem.* **2015**, *54*, 8639–8643.

(25) Wang, H., Lisa J.and Deng; Furukawa, H.; Gandara, F.; Cordova, K. E.; Peri, D.; Yaghi, O. M. Synthesis and Characterization of Metal–Organic Framework-74 Containing 2, 4, 6, 8, and 10 Different Metals. *Inorg. Chem.* **2014**, *53*, 5881–5883.

(26) Ji, Z.; Li, T.; Yaghi, O. M. Sequencing of metals in multivariate metal-organic frameworks. *Science* **2020**, *369*, 674–680.

(27) Panda, T.; Horike, S.; Hagi, K.; Ogiwara, N.; Kadota, K.; Itakura, T.; Tsujimoto, M.; Kitagawa, S. Mechanical Alloying of Metal–Organic Frameworks. *Angew. Chem. Int. Ed.* **2017**, *56*, 2413–2417.

(28) Cliffe, C., Matthew J.and Mottillo; Stein, R. S.; Bučar, D.-K.; Friščić, T. Accelerated aging: a low energy, solvent-free alternative to solvothermal and mechanochemical synthesis of metal–organic materials. *Chem. Sci.* **2012**, *3*, 2495–2500.

(29) Ayoub, G.; Karadeniz, B.; Howarth, A. J.; Farha, O. K.; Đilović, I.; Germann, L. S.; Dinnebier, R. E.; Užarević, K.; Friščić, T. Rational Synthesis of Mixed-Metal Microporous Metal-Organic Frameworks with Controlled Composition Using Mechanochemistry. *Chem. Mater.* **2019**, *31*, 5494–5501.

(30) Stolar, T.; Prašnikar, A.; Martinez, V.; Karadeniz, B.; Bjelić, A.; Mali, G.; Friščić, T.; Likozar, B.; Užarević, K. Scalable Mechanochemical Amorphization of Bimetallic Cu–Zn MOF-74 Catalyst for Selective CO_2 Reduction Reaction to Methanol. *ACS Appl. Mater. Interfaces* **2021**, *13*, 3070–3077.

(31) Canepa, P.; Chabal, Y. J.; Thonhauser, T. When metal organic frameworks turn into linear magnets. *Phys. Rev. B* **2013**, *87*, 094407.

(32) Bloch, E. D.; Queen, W. L.; Krishna, R.; Zadrozny, J. M.; Brown, C. M.; Long, J. R. Hydrocarbon Separations in a Metal-Organic Framework with Open Iron(II) Coordination Sites. *Science* **2012**, *335*, 1606–1610.

(33) Kim, H.; Park, J.; Jung, Y. The binding nature of light hydrocarbons on Fe/MOF-74 for gas separation. *Phys. Chem. Chem. Phys.* **2013**, *15*, 19644–19650.

(34) Park, J.; Kim, H.; Jung, Y. Origin of Selective Guest-Induced Magnetism Transition in Fe/MOF-74. *J. Phys. Chem. Lett.* **2013**, *4*, 2530–2534.

(35) Rubio-Giménez, V.; Waerenborgh, J. C.; Clemente-Juan, J. M.; Martí-Gastaldo, C. Spontaneous Magnetization in Heterometallic NiFe-MOF-74 Microporous Magnets by Controlled Iron Doping. *Chem. Mater.* **2017**, *29*, 6181–6185.

(36) Son, K.; Kim, J. Y.; Schütz, G.; Kang, S. G.; Moon, H. R.; Oh, H. Coordinated Molecule-Modulated Magnetic Phase with Metamagnetism in Metal–Organic Frameworks. *Inorg. Chem.* **2019**, *58*, 8895–8899.

(37) Son, K.; Kim, R. K.; Kim, S.; Schütz, G.; Choi, K. M.; Oh, H. Metal Organic Frameworks as Tunable Linear Magnets. *Phys. Status Solidi A* **2020**, *217*, 1901000.

(38) Muratović, S.; Karadeniz, B.; Stolar, T.; Lukin, S.; Halasz, I.; Herak, M.; Mali, G.; Krupskaya, Y.; Kataev, V.; Žilić, D.; Užarević, K. Impact of dehydration and mechanical amorphization on the magnetic properties of Ni(ii)-MOF-74. *J. Mater. Chem. C* **2020**, *8*, 7132–7142.

(39) Zhao, X.; Pattengale, B.; Fan, D.; Zou, Z.; Zhao, Y.; Du, J.; Huang, J.; Xu, C. Mixed-Node Metal–Organic Frameworks as Efficient Electrocatalysts for Oxygen Evolution Reaction. *ACS Energy Lett.* **2018**, *3*, 2520–2526.

(40) Mukoyoshi, M.; Maesato, M.; Kawaguchi, S.; Kubota, Y.; Cho, K.; Kitagawa, Y.; Kitagawa, H. Systematic Tuning of the Magnetic Properties in Mixed-Metal MOF-74. *Inorg. Chem.* **2022**, *61*, 7226–7230.

(41) Lukin, S.; Germann, L. S.; Friščić, T.; Halasz, I. Toward Mechanistic Understanding of Mechanochemical Reactions Using Real-Time In Situ Monitoring. *Acc. Chem. Res.* **2022**, *55*, 1262–1277.

(42) Užarević, K.; Halasz, I.; Friščić, T. Real-Time and In Situ Monitoring of Mechanochemical Reactions: A New Playground for All Chemists. *J. Phys. Chem. Lett.* **2015**, *6*, 4129–4140.

(43) Hadjiivanov, K. I.; Panayotov, D. A.; Mihaylov, M. Y.; Ivanova, E. Z.; Chakarova, K. K.; Andonova, S. M.; Drenchev, N. L. Power of Infrared and Raman Spectroscopies to Characterize Metal-Organic Frameworks and Investigate Their Interaction with Guest Molecules. *Chem. Rev.* **2021**, *121*, 1286–1424.

(44) Flores, J. G.; Sánchez-González, E.; Gutiérrez-Alejandre, A.; Aguilar-Pliego, J.; Martínez, A.; Jurado-Vázquez, T.; Lima, E.; González-Zamora, E.; Díaz-García, M.; Sánchez-Sánchez, M.; Ibarra, I. A. Greener synthesis of Cu-MOF-74 and its catalytic use for the generation of vanillin. *Dalton Trans.* **2018**, *47*, 4639–4645.

(45) Stoll, S.; Schweiger, A. EasySpin, a comprehensive software package for spectral simulation and analysis in EPR. *J. Magn. Reson.* **2006**, *178*, 42–55.

(46) Blundell, S. *Magnetism in Condensed Matter*; Oxford University Press: Oxford, UK, 2006.

(47) Spaldin, N. A. *Magnetic Materials Fundamentals and Applications*; Cambridge University Press: Cambridge, UK, 2013.

(48) Bonner, J. C.; Fisher, M. E. Linear Magnetic Chains with Anisotropic Coupling. *Phys. Rev.* **1964**, *135*, A640–A658.

(49) Kahn, O. *Molecular Magnetism*; Wiley-VCH Inc., 1993.
(50) Anderson, P. W.; Weiss, P. R. Exchange Narrowing in Paramagnetic Resonance. *Rev. Mod. Phys.* **1953**, *25*, 269–276.
(51) Anderson, P. W. A Mathematical Model for the Narrowing of Spectral Lines by Exchange or Motion. *J. Phys. Soc. Japan* **1954**, *9*, 316–339.
(52) Žilić, D.; Androš, L.; Krupskaya, Y.; Kataev, V.; Büchner, B. Magnetic anisotropy of Cr(III) ions in polymeric oxalate complexes as revealed by HF-ESR spectroscopy. *Appl. Magn. Reson.* **2015**, *46*, 309–321.
(53) Žilić, D.; Molčanov, K.; Jurić, M.; Habjanič, J.; Rakvin, B.; Krupskaya, Y.; Kataev, V.; Wurmehl, S.; Büchner, B. 3D oxalate-based coordination polymers: Relationship between structure, magnetism and color, studied by high-field ESR spectroscopy. *Polyhedron* **2017**, *126*, 120–126.
(54) Androš, L.; Jurić, M.; Popović, J.; Pajić, D.; Krupskaya, Y.; Kataev, V.; Büchner, B.; Žilić, D. Magneto-structural correlations in oxalate-bridged Sr(II)Cr(III) coordination polymers: structure, magnetization, X-band, and high-field ESR studies. *Dalton Trans.* **2018**, *47*, 3992–4000.
(55) Bleaney, B.; Bowers, K. D. Anomalous Paramagnetism of Copper Acetate. *Proc. R. Soc. London, Ser. A* **1952**, *214*, 451.
(56) Mali, G.; Mazaj, M. Hyperfine Coupling Constants in Cu-Based Crystalline Compounds: Solid-State NMR Spectroscopy and First-Principles Calculations with Isolated-Cluster and Extended Periodic-Lattice Models. *J. Phys. Chem. C.* **2021**, *125*, 4655–4664.
(57) Luo, F.; Yan, C.; Dang, L.; Krishna, R.; Zhou, W.; Wu, H.; Dong, X.; Han, Y.; Hu, T.-L.; O'Keeffe, M.; Wang, L.; Luo, M.; Lin, R.-B.; Chen, B. UTSA-74: A MOF-74 Isomer with Two Accessible Binding Sites per Metal Center for Highly Selective Gas Separation. *J. Am. Chem. Soc.* **2016**, *138*, 5678–5684.